ADVANCED THEORY AND SIMULATIONS
www.advtheorysimul.com

Role of Anions in 5-Hydroxymethylfurfural Solvation in Ionic Liquids from Molecular Dynamics Simulations

Hadrián Montes-Campos, Trinidad Méndez-Morales, Luis Miguel Varela, and Manuel Angel Ortuño**

The proper selection of solvents for biomass upgrading is a crucial task as it should carefully balance the enhancement of reactivity with a facile product recovery. A challenging case is the conversion of glucose and fructose to 5-hydroxymethylfurfural (HMF). Ionic liquids (ILs) are often employed to boost the activity and selectivity of this process, although the isolation of HMF from the medium remains a major drawback. To investigate such solvent effects in a realistic (dynamic) environment, classical molecular dynamics (MD) simulations of HMF are performed in imidazolium-based ILs with different anions. Several parameters are identified that directly control HMF–anion interactions, which may hamper product separation, as well as HMF–HMF contacts, which can promote undesired side-reactions. These computational results would guide future high-throughput screenings of new and improved IL media.

1. Introduction

The catalytic valorization of biomass feedstocks into high-value chemicals is a promising strategy to establish a renewable source of carbon atoms that does not rely on fossil fuels.[1] Organic media showed great results in terms of solubility of biobased substrates and chemical transformations.[2] But as development reaches the industrial scale, the use of volatile solvents should be minimized. Ionic liquids (ILs), composed of organic and inorganic ions, are promising alternatives due to their low volatility and nonflammability.[3] Their great versatility and huge chemical space allow us to tune them for almost any particular task, including biomass pretreatment[4] and conversion.[5]

Among the most relevant transformations, we focus on the selective dehydration of sugars, cheap and ready-available substrates, into 5-hydroxymethylfurfural (HMF), a key "top ten" biobased product[6] that gives access to a vast number of chemicals such as plastic monomers and fuels (**Scheme 1**).[7] The reaction network of this process is quite intricate[8] and ILs indeed play a major role controlling both activity and selectivity.[9] For instance, imidazolium-based ILs yielded HMF from fructose,[10] and Cr-based catalysts allowed such conversion directly from glucose while preventing side-reactions such as hydrolysis and oligomerization.[11]

Despite the enhanced catalytic performance of these systems, the separation of the resulting HMF product from the IL medium poses a new challenge as it often requires organic solvents to be efficient, such as glycol dimethyl ether or tetrahydrofuran.[12] Here is where the versatility and tunability of ILs come into play. Al Ghatta et al. reported an increase of one order of magnitude in the partition coefficient in the absence of Cl^- for [OTf]-based ILs,[13] and proposed the use of $[NTf]^-$ anions for HMF separation.[14] Wang et al. observed that the extraction efficiency of ILs with different anions followed the trend $[BF_4]^- > [CH_3SO_3]^- > [CH_3OSO_3]^- > [NO_3]^- > [Cl]^-$.[15] Computational simulations with cluster models suggested that hydrogen bond interactions between HMF and anions are responsible for its difficult separation.[16] However, ILs are complex systems that require a multiscale approach.[17] The use of isolated, nondynamic charged species may result in an oversimplified picture that should be taken with caution when comparing with experimental data. To address this issue, the coordination environment of HMF within bulk liquids must be treated via molecular dynamics (MD) techniques. There exist classical MD studies of HMF in water,[18,19] and DMSO–water mixtures,[18,20] as well as ab initio MD studies of HMF in water.[21] To the best of our knowledge, only one computational report considers HMF in [BMIM][Cl] (1-butyl-3-methyl-imidazolium chloride), but structural information is barely discussed.[22]

H. Montes-Campos, T. Méndez-Morales, L. M. Varela
Grupo de Nanomateriais, Fotónica e Materia Branda
Departamento de Física de Partículas
Universidade de Santiago de Compostela
Campus Vida s/n, Santiago de Compostela 15782, Spain
E-mail: hadrian.montes@usc.es

M. A. Ortuño
Centro Singular de Investigación en Química Biolóxica e Materiais Moleculares (CIQUS)
Universidade de Santiago de Compostela
Campus Vida s/n, Santiago de Compostela 15782, Spain
E-mail: manuelangel.ortuno@usc.es

The ORCID identification number(s) for the author(s) of this article can be found under https://doi.org/10.1002/adts.202200522

DOI: 10.1002/adts.202200522

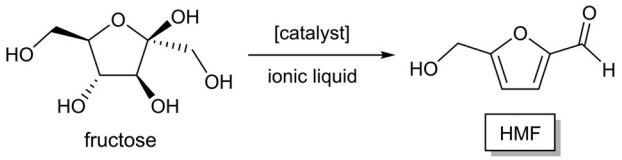

Scheme 1. Catalytic conversion of fructose into 5-hydroxymethylfurfural in ILs.

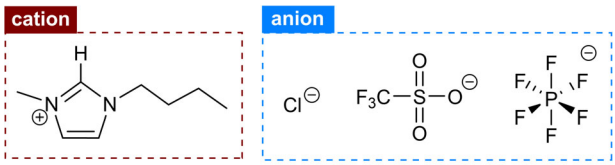

Figure 1. ILs under computational study: [BMIM][Cl], [BMIM][OTf], [BMIM][PF_6].

The current state-of-the-art lacks a comprehensive analysis of coordination environments of furanic compounds in complex IL solutions. In that sense, computational techniques become crucial to gather insight at atomic level of detail, where routine experiments cannot easily access.[23] In this work, we examine the solution behavior of HMF in imidazolium-based ILs by means of classical MD simulations. We consider three systems, consisting of $[BMIM]^+$ and three anions with different coordinating capabilities: $[Cl]^-$, $[OTf]^-$, and $[PF_6]^-$ (**Figure 1**). Our computational approach allows us to i) avoid pitfalls of nondynamic cluster models, ii) unravel solute–solvent and solute–solute interactions under realistic experimental conditions (temperature, concentration, time), and iii) determine specific parameters and trends to guide the design of new IL-based reaction and separation media.

2. Results and Discussion

The typical set-up model for the systems under study is presented in **Figure 2**a. It contains 300 HMF molecules and 5700 IL pairs, giving a molar fraction of 5% as reported in experiments.[13] At such low concentration, we do not expect major changes in the behavior of the ILs, and thus we focus our analysis on HMF and its surroundings. In the next sections, we will refer to particular atoms of the solute (HMF) following the nomenclature in Figure 2b, where O1 stands for the furan, O2 for the alcohol, and O3 for the aldehyde O atoms. We will separately analyze the interactions of the solute with cations, anions, and other solute molecules. Finally, we discuss the implications of each IL in the solvation of HMF and identify parameters to drive future screening studies aiming to balance selectivity and separability.

2.1. Solute–Cation Interactions

We first analyze the contacts between HMF and $[BMIM]^+$ for all systems by means of radial distribution functions (RDFs). These functions, also denoted as $g(r)$, represent the probability of finding a target entity (an atom, a group, or a molecule) at a certain

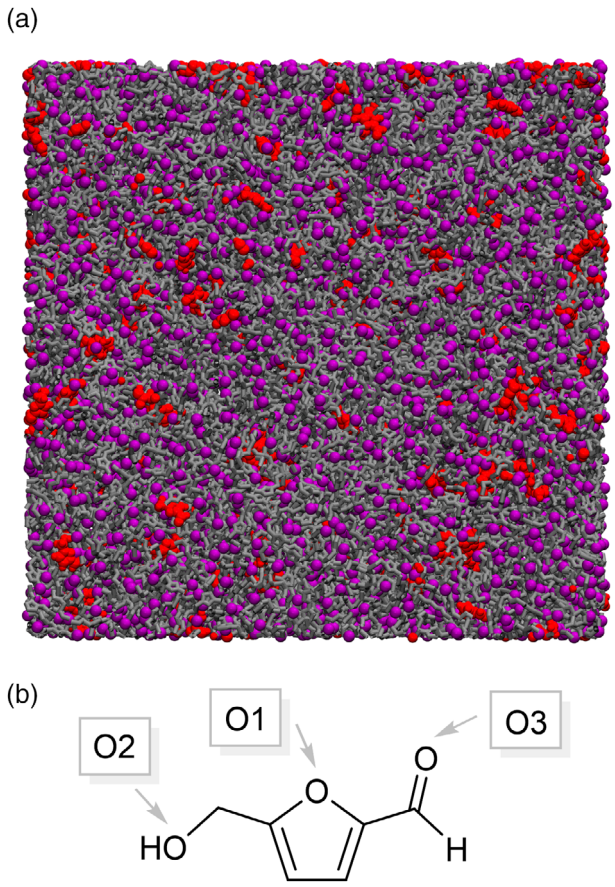

Figure 2. a) Fully atomistic computational model of 300 HMF molecules dissolved in 5700 IL pairs ([BMIM][Cl] as example). Cations are represented in gray (wire model), anions in purple, and HMF molecules in red. b) Nomenclature of oxygen atoms in HMF.

distance from a reference entity along the simulation time. The RDFs are normalized in such way that a value of 1 corresponds to a random distribution of target entities. Therefore, values greater than 1 indicate an attractive interaction and a value lower than 1 a repulsive one. **Figure 3** shows the RDFs between the three O atoms in HMF (reference) and the centroid of the imidazolium ring of the cation (target) for the three IL solvents. For [BMIM][Cl] (green), all three O atoms are typically found at ≈0.4 nm from the cation. Interestingly, the other ILs [BMIM][OTf] (orange) and [BMIM][PF_6] (blue) behave in the same way. Thus, despite minor differences, all systems present similar HMF–cation patterns, indicating that the type of anion has little impact on this aspect. Cations are mainly spectator species[24] and their interaction with HMF is indeed expected to be weaker than that with anions (Figure S1, Supporting Information).[25]

2.2. Solute–Anion Interactions

We next consider the solvation pattern of HMF with respect to the different anions. **Figure 4** shows the RDFs between the three O atoms in HMF and the central atom of the anions (Cl for $[Cl]^-$, S for $[OTf]^-$, and P for $[PF_6]^-$) for the three IL solvents. For [BMIM][Cl] (green), O1 and O3 barely interact with them, having

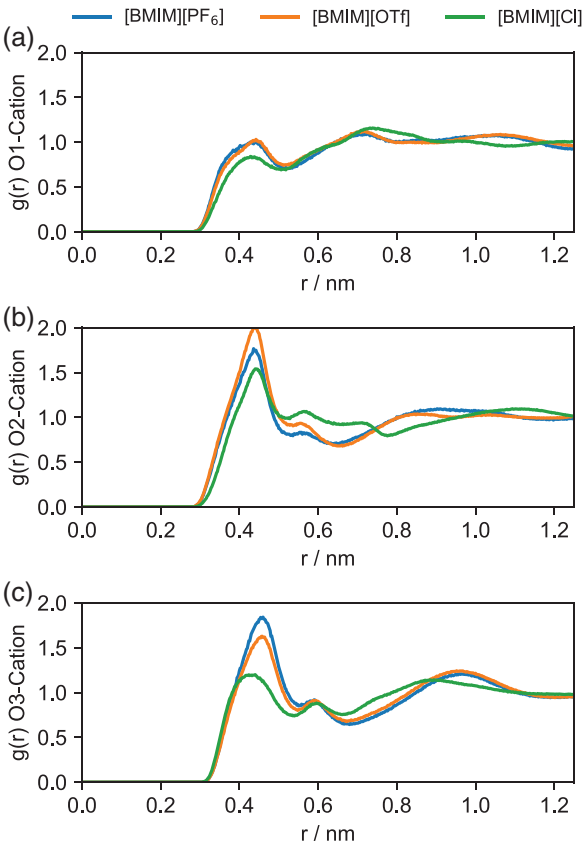

Figure 3. Radial distribution functions (RDFs) between the different O atoms of HMF and the cation. Distances in nm.

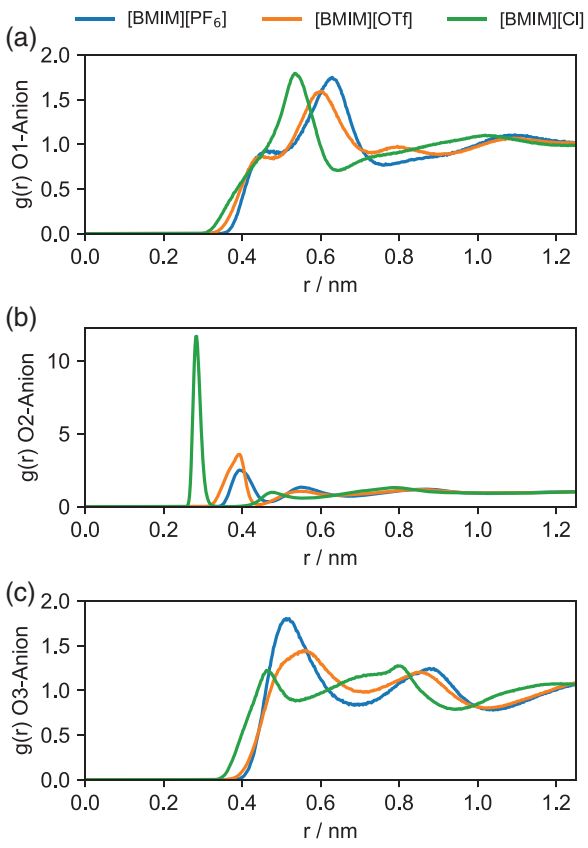

Figure 4. Radial distribution functions (RDFs) between the different O atoms of HMF and the anions. Distances in nm.

main peaks at ≈0.4 and 0.5 nm, respectively. However, the coordination around O2 is completely distinct as the alcohol group can act as hydrogen bond donor. We observe a very strong attractive interaction with a sharp peak at ≈0.3 nm. In the systems [BMIM][OTf] (orange) and [BMIM][PF_6] (blue), O1 and O3 also show less attraction. O2 again behaves differently from O1 and O3, displaying sharper peaks at ≈0.4 nm. Those peaks are displaced with respect to that from [BMIM][Cl] due to the different ion size.

We also compute the spatial distribution functions (SDFs), which are the 3D extension of the RDFs. **Figure 5** represents the isosurfaces of the HMF–anion SDFs with a probability higher than 15 times the homogeneous distribution. For O2, all anions show a well-defined interaction region next to the hydrogen of the alcohol group. As for O3, direct contacts with the anions are not found. However, the hydrogen of the aldehyde group (which has a slightly positive charge) displays a high probability region for $[Cl]^-$ and $[PF_6]^-$ but not for $[OTf]^-$. This could be related with a lower charge density in $[OTf]^-$ compared to the other smaller anions.

The different coordination patterns of O2 require further discussion. As mentioned before, all anions show a preferential interaction with O2; however, the strength of such attraction is highly dependent on the nature of the anion, as reported for cellulose.[26] The strongest interaction occurs with $[Cl]^-$, whose peak reaches a high intensity of 11.5. The systems containing

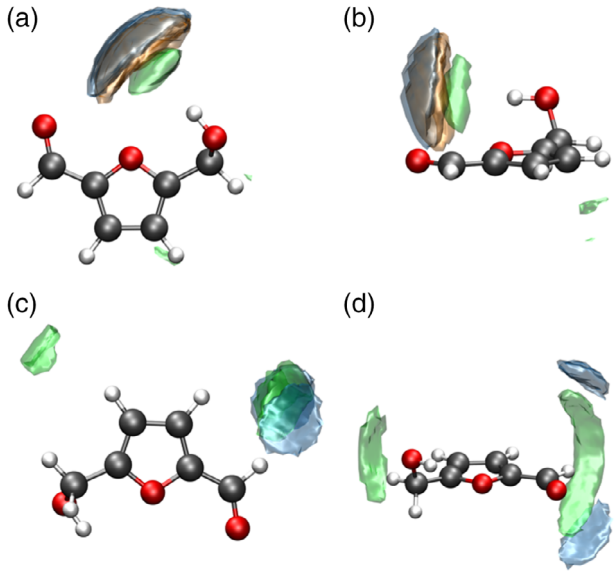

Figure 5. Isosurfaces of spatial distribution functions (SDFs) with a probability of 15 times the random distribution of anions around HMF; (a) and (b) show the top and side views of the high probability regions surrounding O2, while (c) and (d) show the same for O3. $[Cl]^-$ in green, $[OTf]^-$ in orange, and $[PF_6]^-$ in blue.

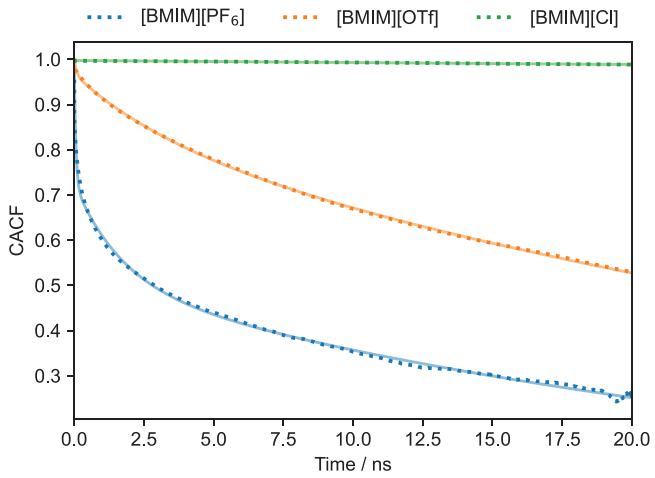

Figure 6. Cage autocorrelation functions (CACFs) between the O2 atom of HMF and the anions. Time in ns. Raw data in dash lines, fitting functions in solid lines.

$[OTf]^-$ and $[PF_6]^-$ show lower peaks with intensities of 3.6 and 2.5, respectively. These values can actually be used to estimate the binding energy using the potential of the mean force (ω_{12}), which is calculated as

$$\omega_{12}\ (r) = -k_B T \log\left(g\,(r)\right) \tag{1}$$

Using this expression, the binding energy between HMF and $[Cl]^-$ is estimated as 2.5 times the thermal energy ($k_B \cdot T$). Following the same procedure, the binding energy for HMF and $[OTf]^-$ is 1.3 times the thermal energy, while for HMF and $[PF_6]^-$ is 0.9 times the thermal energy. Therefore, we expect the coordination of HMF to $[Cl]^-$ to be resilient in time, while that involving $[OTf]^-$ would be more transient. A similar observation was noted in MD simulations with fructose, where $[OTf]^-$ binds weaker to it[27] or migrates away from it.[28] On the other hand, the species HMF–$[PF_6]^-$ has a binding energy lower than the thermal energy, and it would be quite labile.

The coordination strength between different anions is further analyzed by calculating the cage autocorrelation function (CACF), which is defined as

$$\text{CACF}\ (\Delta t) = \frac{\langle \theta_{i,j}\,(t)\,\theta_{i,j}\,(t+\Delta t)\rangle}{\langle \theta_{i,j}\,(t)\,\theta_{i,j}\,(t)\rangle} \tag{2}$$

where $\langle\ \rangle$ represents the ensemble average and $\theta_{i,j}(t)$ is a function that takes the value 1 if a pair of atoms i,j is closer than a given coordination distance and 0 if the atoms are further away. The first minimum of the RDF was used as the coordination distance. This expression creates a cage of radius X around a reference entity (O2) over a period of time and evaluates whether the selected entities (anions) are inside (value of 1) or outside (value of 0). **Figure 6** shows the CACFs of the O2 atom during 20 ns for the three IL systems. We can see that $[Cl]^-$ stays in the surroundings of O2 for the entire inspected time, while $[OTf]^-$ and particularly $[PF6]^-$ start to leave the coordination sphere of O2 after several ns.

Table 1. Intensity and mean time parameters (fitting values) for CACFs.

Stage	Parameter	$[Cl]^-$	$[OTf]^-$	$[PF_6]^-$
(1)[a]	Intensity [%]	–	3%	27%
	Mean time [ps]	–	88.7	57.2
(2)[b]	Intensity [%]	100%	13%	22%
	Mean time [ns]	2.1×10^6	3.5	1.7
(3)[c]	Intensity [%]	–	84%	51%
	Mean time [μs]	–	43	29

[a] Pre-complex dissociation; [b] Complex lifetime; [c] Complex regeneration.

We can fit these correlations to a triple exponential, similar to the one usually used for describing hydrogen bond correlations.[29] The three exponentials are associated to different binding stages: (1) is a fast process where the complex is not completely formed and breaks very fast, (2) is a process that represents the average continuous lifetime of a complex and its subsequent dissociation, and (3) is a slow process that takes into account multiple regenerations of the complex. The results for the fitting and their corresponding stages are collected in **Table 1**. We note that the accuracy of the mean time measurements quickly decreases once the mean time is larger than the simulation time (40 ns) and, therefore, the values for longer times (such as microseconds) must be taken as rough estimations. On the one hand, HMF–$[Cl]^-$ has a large lifetime (2), even reaching the microsecond scale. There is no contribution due to fast pre-complex dissociation (1) and slow complex regeneration (3), thus this interaction is quite persistent in time and complex dissociation would occur in a longer time scale. On the other hand, HMF–$[OTf]^-$ and HMF–$[PF_6]^-$ have similar and smaller lifetimes of 3.5 and 1.7 ns, respectively. For $[OTf]^-$ there is a major part (84%) that concerns multiple regenerations of the complex (3). Interestingly, for $[PF_6]^-$ there is a significant contribution (27%) of the pre-complex dissociation (1), which is related to the average binding energy being slightly lower than the thermal energy.

We also analyzed the surface coverage of HMF via Voronoi analysis, from which we obtain the amount of neighboring target entities around our HMF reference (Figure S2, Supporting Information). Although no clear conclusions could be drawn due to the different size of the anions, the data already imply the nearby presence of HMF molecules around HMF, which is analyzed in the next section.

2.3. Solute–Solute Interactions

Although the solute is mostly in contact with solvent molecules at low concentration (molar fraction of 5%), HMF–HMF interactions must also be considered because they can lead to undesired side-products under typical reaction conditions. **Figure 7** shows the RDFs between O2 atoms belonging to different HMF molecules for the three IL systems (for RDFs with O1 and O3 atoms, see Figure S3, Supporting Information). For [BMIM][Cl] (green), there is no clear interaction between oxygen atoms, showing a relatively small peak at ≈0.5 nm. On the other hand, both [BMIM][OTf] (orange) and [BMIM][PF_6] (blue) display peaks at shorter distances of ≈0.3 nm although with quite different intensity. While this contact is rather uncommon for the former, it

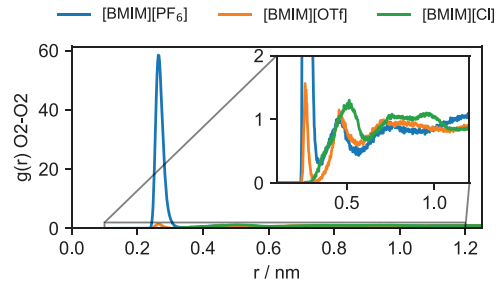

Figure 7. Radial distribution functions (RDFs) between the O2 atoms of HMF molecules. Distances in nm.

is extremely important for the latter. This is the result of a strong hydrogen bond interaction between two OH groups (one acting as donor and another one as acceptor).

As indicated above, the main HMF–HMF interaction mechanism is the formation of hydrogen bonds between alcohol groups (O2). However, the extent of such contacts is deeply linked to the nature of the anion in the IL. That is, anions can compete with HMF molecules for the coordination to O2, and they could even prevent HMF association.

According to previous HMF–anion binding energies, we expect the number of solute–solute hydrogen bonds to increase from $[Cl]^-$ to $[OTf]^-$ and $[PF_6]^-$. To support this hypothesis, we calculate the number of hydrogen bonds per HMF molecule for the three systems, as shown in **Figure 8**a. For [BMIM][PF_6], we observe a significant number of hydrogen bonds between HMF molecules (≈1 hydrogen bond per 10 molecules), mostly through the O2 atoms. This is remarkable because the concentration of HMF is low. Interestingly, there is a drastic reduction in the number of hydrogen bonds (≈97%) when changing the anion to $[OTf]^-$. For [BMIM][Cl], the number of hydrogen bonds between HMF molecules is negligible. The ability of $[OTf]^-$ and $[Cl]^-$ to prevent the aggregation of HMF molecules is further demonstrated by calculating the distribution of HMF cluster sizes, as shown in Figure 8b. For $[PF_6]^-$, we can see a larger number of HMF pairs. Although HMF seems to aggregate in larger groups with $[Cl]^-$ and $[OTf]^-$ (>3 molecules), this is just a result of a non-interactive spatial proximity since hydrogen bond interactions between HMF molecules are not observed (Figure 8a and Figure S4, Supporting Information). Indeed, the key role that O2 has in our simulations is in line with recent experiments, where the substitution of OH by OMe in HMF resulted in fewer side-products (humins) and easier separations.[30]

2.4. Overall Solvation Scenario

Merging together all previous insight about solute–cation, solute–anion, and solute–solute interactions, we suggest the following solvation picture for HMF in ILs. First, cations behave as spectator species with respect to HMF. Second, anions bind to HMF with different strength depending on their coordinating nature, which in turn impacts solute–solute interactions. The balance of both terms is key as strong HMF–anion species hamper separation and strong HMF–HMF ones lead to side-reactions.

In that regard, our simulations allow us to measure the extent and dominance of these processes through quantitative parameters. Instead of typical binding energies obtained from charged, finite-size cluster models, which neglect the bulk liquid environment, we here present the following descriptors obtained from dynamic approaches: lifetime of the complex between solute and IL anions via CACFs and degree of association between solute molecules via hydrogen bond counting. These parameters would help to evaluate the potential of an IL to adequately solvate HMF while preventing its self-aggregation. This strategy establishes reliable guidelines from where to perform screenings across libraries of IL and mixed IL media.

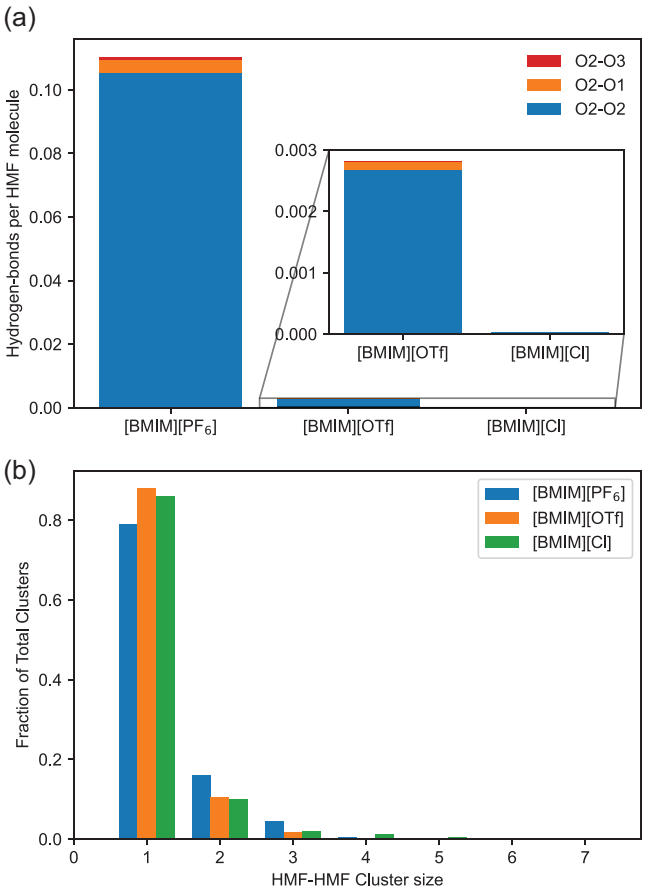

Figure 8. a) Number of hydrogen bonds per HMF molecule for the different anions. b) Histogram of HMF cluster sizes for the different anions.

3. Conclusions

Here we report a detailed analysis of the solvent effects of ionic liquids on the biomass-relevant HMF product through classical MD simulations. We study several systems containing the same cation and three anions with different coordinating strengths: [BMIM][Cl], [BMIM][OTf], and [BMIM][PF_6]. While the cations are mostly spectators, the anions bind to HMF with strengths following the trend $[Cl]^-$ >> $[OTf]^-$ > $[PF_6]^-$. Such behavior implies that HMF–HMF interactions follow the opposite trend $[PF_6]^-$ >> $[OTf]^-$ > $[Cl]^-$. In line with experimental evidence, our simulations indicate that: [BMIM][Cl] hampers the isolation of HMF and [BMIM][PF_6] favors HMF self-interaction which may lead to side-reactions, [BMIM][OTf] laying in between both previous cases.

From these results we propose two key descriptors to quantitatively described the behavior of HMF in IL media: the lifetime of HMF–anion complexes and the degree of HMF–HMF aggregation. Our dynamic approach will help guide the design of new reaction media for the conversion of biomass resources into high-value feedstocks, pursuing not only improved selectivity but also easy product separation.

4. Experimental Section

Computational Details: Classical molecular dynamics (MD) simulations were performed using the GROMACS 2019.5 package[31] with the nonpolarizable OPLS-AA force field,[32] which includes all the atoms present in the systems and does not account for the electronic polarization. These nonpolarizable force fields can predict the correct structure and a qualitatively correct dynamics with a fraction of the computational cost of the polarizable ones.[33] The topologies for each species were obtained from reported literature: $[BMIM]^+$ and $[PF_6]^-$ from,[32] $[OTf]^-$ from,[34] and HMF from.[35] Values of the Lennard–Jones (LJ) parameters for $[Cl]^-$ are $\sigma = 3.77 \times 10^{-1}$ Å and $\epsilon = 6.2012 \times 10^{-1}$ kJ mol^{-1}.[36] The total charge of the ionic species was set to ±1e (i.e., the charges were not scaled).

The PACKMOL software[37] was employed to obtain the initial configurations in which the molecules were randomly distributed inside the cubic simulation box. Then, the energy of the systems was minimized using a conjugate gradient algorithm. The maximum step size and the tolerance were set to 0.01 nm and 0.1 kJ nm^{-1} mol^{-1}, respectively. This was followed by stabilization (for 20 ns) of the systems in the isothermal-isobaric (NpT) ensemble to reach the experimental density at $T = 298.15$ K and $p =$ 1 atm. The temperature was controlled using the V-rescale thermostat introduced by Bussi et al.[38] with a coupling constant of 0.1 ps, whereas the pressure was kept constant with the Parrinello–Rahman barostat[39] with an isothermal compressibility of 4.5×10^{-5} bar^{-1} and a relaxation time of 1 ps. Finally, the results of an additional 40 ns–long simulation in the same ensemble were used for the structural analysis of the mixtures. The time step of the simulations was 1 fs and periodic boundary conditions were applied in all directions. Long-range electrostatic interactions were treated by using the Particle Mesh Ewald (PME) method[40] with a grid spacing of 0.12 nm and cubic interpolation. A cut-off distance of 1.1 nm was used for both Coulomb and LJ interactions. The geometric average was used for the combination rules of both LJ parameters.[41] The Linear Constraint Solver (LINCS) algorithm,[42] with a fourth order expansion of the constraint coupling matrix, was used to fix all the bond lengths with H atoms. Voronoi analyses were performed with the trajectory analyzer software TRAVIS.[43] For the hydrogen bond count, the threshold distance donor–acceptor was set to 0.35 nm and the threshold angle hydrogen–donor–acceptor was set to less than 30°.

Each of these simulations provided us a sequence of configurations, i.e., positions and instantaneous velocities of all atoms of the mixtures, which were analyzed to obtain structural information about the aforementioned systems.

Supporting Information

Supporting Information is available from the Wiley Online Library or from the author.

Acknowledgements

This work was funded by the Spanish Ministry of Economy and Competitiveness (under projects MAT2017-89239-C2-1-P and PID2020-119116RA-I00) and by the Xunta de Galicia (ED431D 2017/06, ED431E 2018/08, GRC ED431C 2016/001, and GRC ED431C 2020/10). All these projects were partially supported by FEDER. H.M.C. thanks the USC for his "Convocatoria de Recualificación do Sistema Universitario Español-Margarita Salas" postdoctoral grant under the "Plan de Recuperación Transformación" program funded by the Spanish Ministry of Universities with European Union's NextGenerationEU funds. T.M.M. acknowledges her contract funded by the pilot program of the USC for the recruitment of distinguished research personnel—call 2021 under the agreement between the USC and the Santander Bank for 2021–2024. M.A.O. acknowledges the Xunta Distinguished Researcher program (ED431H 2020/21), the Xunta de Galicia (Centro singular de investigación de Galicia accreditation 2019–2022, ED431G 2019/03), and the European Union (European Regional Development Fund – ERDF) for funding. He also acknowledges CESGA ("Centro de Supercomputación de Galicia") for providing computational resources.

Conflict of Interest

The authors declare no conflict of interest.

Data Availability Statement

The data that support the findings of this study are available from the corresponding author upon reasonable request.

Keywords

biomass, hydrogen bonds, ionic liquids, molecular dynamics, solvent effects

Received: July 22, 2022
Revised: September 3, 2022
Published online: October 9, 2022

[1] C. O. Tuck, E. Pérez, I. T. Horváth, R. A. Sheldon, M. Poliakoff, *Science* **2012**, *337*, 695.
[2] L. Shuai, J. Luterbacher, *ChemSusChem* **2016**, *9*, 133.
[3] J. P. Hallet, T. Welton, *Chem. Rev.* **2011**, *111*, 3508.
[4] H. Tadesse, R. Luque, *Energy Environ. Sci.* **2011**, *4*, 3913.
[5] a) Z. Zhang, J. Song, B. Han, *Chem. Rev.* **2017**, *117*, 6834; b) A. Salama, P. Hesemann, *ACS Sustainable Chem. Eng.* **2020**, *8*, 17893.
[6] J. J. Bozell, G. R. Petersen, *Green Chem.* **2010**, *12*, 539.
[7] a) R. J. Van Putten, J. C. Van Der Waal, E. De Jong, C. B. Rasrendra, H. J. Heeres, J. G. De Vries, *Chem. Rev.* **2013**, *113*, 1499; b) C. Xu, E. Paone, D. Rodríguez-Padrón, R. Luque, F. Mauriello, *Chem. Soc. Rev.* **2020**, *49*, 4273; c) Q. Hou, X. Qi, M. Zhen, H. Qian, Y. Nie, C. Bai, S. Zhang, X. Bai, M. Ju, *Green Chem.* **2021**, *23*, 119; d) F. Chacón-Huete, C. Messina, B. Cigana, P. Forgione, *ChemSusChem* **2022**, *15*, 202200328.
[8] L. Zhu, X. Fu, Y. Hu, C. Hu, *ChemSusChem* **2020**, *13*, 4812.
[9] a) M. E. Zakrzewska, E. Bogel-Łukasik, R. Bogel-Łukasik, *Chem. Rev.* **2011**, *111*, 397; b) T. Stahlberg, W. Fu, J. M. Woodley, A. Riisager, *ChemSusChem* **2011**, *4*, 451; c) C. B. T. L. Lee, T. Y. Wu, *Renewable Sustainable Energy Rev.* **2021**, *137*, 110172.
[10] C. Moreau, A. Finiels, L. Vanoye, *J. Mol. Catal. A: Chem.* **2006**, *253*, 165.
[11] a) H. Zhao, J. E. Holladay, H. Brown, Z. C. Zhang, *Science* **2007**, *316*, 1597; b) S. Siankevich, Z. Fei, R. Scopelliti, G. Laurenczy, S. Katsyuba, N. Yan, P. J. Dyson, *ChemSusChem* **2014**, *7*, 1647; c) L. Zhou, Y. He, Z. Ma, R. Liang, T. Wu, Y. Wu, *Carbohyd. Polym.* **2015**, *117*, 694.
[12] J. Zhou, Z. Xia, T. Huang, P. Yan, W. Xu, Z. Xu, J. Wang, Z. C. Zhang, *Green Chem.* **2015**, *17*, 4206.
[13] A. Al Ghatta, J. D. E. T. Wilton-Ely, J. P. Hallett, *ChemSusChem* **2019**, *12*, 4452.

[14] A. Al Ghatta, J. D. E. T. Wilton-Ely, J. P. Hallett, *ACS Sustainable Chem. Eng.* **2019**, *7*, 16483.
[15] H. Wang, J. Cui, Y. Zhao, Z. Li, J. Wang, *Green Chem.* **2021**, *23*, 405.
[16] H. Wang, S. Liu, Y. Zhao, H. Zhang, J. Wang, *ACS Sustainable Chem. Eng.* **2016**, *4*, 6712.
[17] a) B. Kirchner, O. Hollóczki, J. N. Canongia Lopes, A. A. H. Pádua, *Wiley Interdiscip. Rev.: Comput. Mol. Sci.* **2015**, *5*, 202; b) B. Kirchner, J. Blasius, V. Alizadeh, A. Gansäuer, O. Hollóczki, *J. Phys. Chem. B* **2022**, *126*, 766.
[18] S. H. Mushrif, S. Caratzoulas, D. G. Vlachos, *Phys. Chem. Chem. Phys.* **2012**, *14*, 2637.
[19] F. Grote, I. Ermilova, A. P. Lyubartsev, *J. Phys. Chem. B* **2018**, *122*, 8416.
[20] J. C. V. Calderón, S. Jiang, S. H. Mushrif, *ChemPhysChem* **2021**, *22*, 2222.
[21] V. Choudhary, S. H. Mushrif, C. Ho, A. Anderko, V. Nikolakis, N. S. Marinkovic, A. I. Frenkel, S. I. Sandler, D. G. Vlachos, *J. Am. Chem. Soc.* **2013**, *135*, 3997.
[22] J. Zhou, T. Huang, Y. Zhao, Z. Xia, Z. Xu, S. Jia, J. Wang, Z. C. Zhang, *Ind. Eng. Chem. Res.* **2015**, *54*, 7977.
[23] J. J. Varghese, S. H. Mushrif, *React. Chem. Eng.* **2019**, *4*, 165.
[24] J. Lia, Y. Yang, D. Zhang, *Chem. Phys. Lett.* **2019**, *723*, 175.
[25] H. Wang, J. Cui, H. Li, Y. Zhao, J. Wang, *J. Mol. Struct.* **2019**, *1179*, 57.
[26] Y. Zhao, X. Liu, J. Wang, S. Zhang, *Carbohydr. Polym.* **2013**, *94*, 723.
[27] C. Shi, Y. Zhao, J. Xin, J. Wang, X. Lu, X. Zhang, S. Zhang, *Chem. Commun.* **2012**, *48*, 4103.
[28] M. A. Mellmer, C. Sanpitakseree, B. Demir, K. Ma, W. A. Elliott, P. Bai, R. L. Johnson, T. W. Walker, B. H. Shanks, R. M. Rioux, M. Neurock, J. A. Dumesic, *Nat. Commun.* **2019**, *10*, 1132.
[29] R. J. Gowers, P. Carbone, *J. Chem. Phys.* **2015**, *142*, 224907.
[30] Z. Xu, Y. Yang, P. Yan, Z. Xia, X. Liu, Z. C. Zhang, *RSC Adv.* **2020**, *10*, 34732.
[31] a) H. J. C. Berendsen, D. van der Spoel, R. van Drunen, *Comput. Phys. Commun.* **1995**, *91*, 43; b) D. van der Spoel, E. Lindahl, B. Hess, G. Groenhof, A. E. Mark, H. J. C. Berendsen, *J. Comp. Chem.* **2005**, *26*, 1701; c) M. J. Abraham, T. Murtola, R. Schulz, S. Páll, J. C. Smith, B. Hess, E. Lindahl, *SoftwareX* **2015**, *1–2*, 19.
[32] a) W. L. Jorgensen, J. Tirado-Rives, *J. Am. Chem. Soc.* **1988**, *110*, 1657; b) S. V. Sambasivarao, O. Acevedo, *J. Chem. Theory Comput.* **2009**, *5*, 1038.
[33] V. Lesch, H. Montes-Campos, T. Méndez-Morales, L. J. Gallego, A. Heuer, C. Schröder, L. M. Varela, *J. Chem. Phys.* **2016**, *145*, 204507.
[34] J. N. Canongia Lopes, A. A. H. Pádua, *J. Phys. Chem. B* **2004**, *108*, 16893.
[35] R. Xiong, M. León, V. Nikolakis, S. I. Sandler, D. G. Vlachos, *ChemSusChem* **2013**, *7*, 236.
[36] B. Doherty, X. Zhong, S. Gathiaka, B. Li, O. Acevedo, *J. Chem. Theory Comput.* **2017**, *13*, 6131.
[37] L. Martínez, R. Andrade, E. G. Birgin, J. M. Martínez, *J. Comput. Chem.* **2009**, *30*, 2157.
[38] G. Bussi, D. Donadio, M. Parrinello, *J. Chem. Phys.* **2007**, *126*, 014101.
[39] a) M. Parrinello, A. Rahman, *Phys. Rev. Lett.* **1980**, *45*, 1196; b) M. Parrinello, A. Rahman, *J. Appl. Phys.* **1981**, *52*, 7182.
[40] T. Darden, D. York, L. Pedersen, *J. Chem. Phys.* **1993**, *98*, 10089.
[41] R. J. Good, C. J. Hope, *J. Chem. Phys.* **1971**, *55*, 111.
[42] B. Hess, *J. Chem. Theory Comput.* **2008**, *4*, 116.
[43] a) M. Brehm, B. Kirchner, *J. Chem. Inf. Model.* **2011**, *51*, 2007; b) M. Brehm, M. Thomas, S. Gehrke, B. Kirchner, *J. Chem. Phys.* **2020**, *152*, 164105.